



**HAL**  
open science

# Parameterization Analysis in Elastic Full-Waveform Inversion of Multi-Component Seismic Data

Jian Cao, Romain Brossier, Ludovic Métivier

► **To cite this version:**

Jian Cao, Romain Brossier, Ludovic Métivier. Parameterization Analysis in Elastic Full-Waveform Inversion of Multi-Component Seismic Data. 83rd EAGE Annual Conference & Exhibition, Jun 2022, Madrid, Spain. pp.1-5, 10.3997/2214-4609.202210274 . hal-03852657

**HAL Id: hal-03852657**

**<https://hal.science/hal-03852657>**

Submitted on 15 Nov 2022

**HAL** is a multi-disciplinary open access archive for the deposit and dissemination of scientific research documents, whether they are published or not. The documents may come from teaching and research institutions in France or abroad, or from public or private research centers.

L'archive ouverte pluridisciplinaire **HAL**, est destinée au dépôt et à la diffusion de documents scientifiques de niveau recherche, publiés ou non, émanant des établissements d'enseignement et de recherche français ou étrangers, des laboratoires publics ou privés.

# Parameterization analysis in elastic full-waveform inversion of multi-component seismic data

J. Cao<sup>1\*</sup>, R. Brossier<sup>1</sup>, L. Métivier<sup>1,2</sup>

<sup>1</sup> Univ. Grenoble Alpes, ISTerre, F-38058 Grenoble, France

<sup>2</sup> CNRS, Univ. Grenoble Alpes, LJK, F-38058 Grenoble, France

Wednesday 12<sup>th</sup> January, 2022

## Main objectives

This study analyses the influence of different model parameterizations in the elastic full-waveform inversion of multi-component ocean-bottom seismic data, so as to design an effective FWI workflow to reconstruct P- and S-wave velocity models of the subsurface jointly and robustly, applicable in scenarios of both weak and strong elastic effects.

## New aspects covered

We analyse the pros and cons of three different model parameterizations in the elastic full-waveform inversion and build hierarchical FWI workflows over different parameter classes and data components for multi-component ocean-bottom seismic data. Poisson's ratio is used as the indicator to design the overburden models that produce elastic effects varying from weak to strong in the robustness test of the proposed inversion workflows. An effective hierarchical elastic FWI workflow is found for reconstructing P- and S-wave velocity models jointly and robustly in scenarios of both weak and strong elastic effects.

## **Summary (200 words)**

In marine surveys, multi-component seismic data can be acquired by placing 4-component sensors (hydrophone plus three-component geophone) on the seafloor. One benefit of such acquisitions is the source-receiver decoupling which makes it possible to increase the maximum offset and azimuth coverage. Another one is the direct S-wave recording through geophones that offers the possibility to better measure the elastic properties for lithology and reservoir characterization. Multi-parameter elastic full-waveform inversion (FWI) is a promising technique to reconstruct P- ( $V_p$ ) and S-wave velocity ( $V_s$ ) models jointly. Its success depends upon several factors, and one is the choice of the subsurface parameterization over proper data components. This study analyses three different elastic model parameterizations in terms of data sensitivity and model gradient feature. A fluid-solid coupled time-domain FWI engine is employed for an accurate modelling of the acoustic and elastic wavefields in the water and subsurface, respectively. FWI tests are performed on a series of overburden models with increasing elastic effects and a realistic synthetic model, revealing a robust and reliable  $V_p$  and  $V_s$  reconstruction can be achieved by inverting hydrophone data with ( $V_p$ ,  $V_p/V_s$  ratio) parameterization first and then three-component geophone data with ( $V_p$ ,  $V_s$ ) parameterization in a two-step workflow.

## Parameterization analysis in elastic full-waveform inversion of multi-component seismic data

### Introduction

A quantitative estimation of elastic properties from seismic data is crucial for subsurface lithology and reservoir characterization. The  $V_p/V_s$  ratio is usually used for identifying fluid type and estimating porosity and saturation in hydrocarbon reservoirs through several empirical relationships (Hamada, 2004). Full-waveform inversion (FWI) has been proposed for extracting high-resolution quantitative physical parameters of the subsurface by fitting the full information in the seismogram. In marine exploration, FWI is mostly used to derive P-wave velocity models in the acoustic approximation (anisotropy/attenuation potentially as passive parameters) using hydrophone or vertical component data.

Ocean-bottom acquisitions give access to multi-component seismic data by placing 4C sensors (hydrophone plus 3C geophone) on the seafloor. Elastic effects can thus be easily captured through the direct recording of S waves by 3C geophones, especially in the horizontal components. Reconstructing P- and S-wave velocity models jointly needs the use of multi-parameter FWI based on an elastic wave modelling solver. Besides the computational cost challenge, the strong nonlinearity and parameter trade-offs in multi-parameter elastic FWI make a suitable data- and model-driven workflow become necessary (Sears et al., 2010; Wang et al., 2021). To maintain the efficiency and accuracy, our elastic FWI study is performed with a fluid-solid coupled modelling solver, based on the acoustic-elastic coupled wave equation and spectral-element discretization. To reconstruct reliable P- and S-wave velocity models, we build a robust hierarchical FWI workflow applicable in both weak and strong elastic-effect scenarios, through analysing the data sensitivity and model gradient corresponding to different model parameterizations.

### 3D fluid-solid coupled elastic FWI and model parameterization

We define the misfit function in the FWI of multi-component seismic data as

$$J(\mathbf{m}) = \frac{1}{2} \sum_{shots} (\lambda \|\mathbf{d}_p^{syn}(\mathbf{m}) - \mathbf{d}_p^{obs}\|^2 + (1 - \lambda) \|\mathbf{d}_u^{syn}(\mathbf{m}) - \mathbf{d}_u^{obs}\|^2), \quad (1)$$

where  $\mathbf{m}$  denotes the set of subsurface model parameters,  $\mathbf{d}_p^{obs}$  and  $\mathbf{d}_u^{obs}$  are observed hydrophone and 3C geophone data, respectively, and their corresponding synthetic data  $\mathbf{d}_p^{syn}$  and  $\mathbf{d}_u^{syn}$  can be modelled by a 3D fluid-solid coupled elastic modelling solver (Cao et al., 2021).  $\lambda$  takes the value 0 or 1 to decide which data type is inverted. The minimization of  $J(\mathbf{m})$  requires access to the gradient of  $J(\mathbf{m})$  obtained from the zero-lag correlation of the incident and adjoint wavefields.

Seismic velocity ( $V_p, V_s$ ) is a common used model parameterization in elastic FWI (Sears et al., 2010). Based on their gradients and the chain rule, we can derive the gradient expressions with respect to  $V_p/V_s$  ratio ( $R$ ) and Poisson's ratio ( $\sigma$ ) to explore two alternative model parameterizations ( $V_p, R$ ) and ( $V_p, \sigma$ ):

$$\frac{\partial J(\mathbf{m})}{\partial R} = V_s \left( \frac{\partial J(\mathbf{m})}{\partial V_p} - \frac{\partial J(\mathbf{m})}{\partial V_s} \frac{1}{R} \right), \quad \frac{\partial J(\mathbf{m})}{\partial \sigma} = V_s \left( \frac{\partial J(\mathbf{m})}{\partial V_p} - \frac{\partial J(\mathbf{m})}{\partial V_s} \frac{1}{R} \right) / \left( 4 \sqrt{\frac{1-\sigma}{0.5-\sigma}} (0.5 - \sigma)^2 \right). \quad (2)$$

To analyse the data sensitivity in different model parameterizations, we calculate radiation patterns of the partial derivative wavefield modulus associated with one parameter perturbation point in the center of a 2D model. As shown in Figure 1, variations of the calculated modulus in different diffraction modes (P-P, P-S, S-P and S-S) reveal how a specific model parameter can be inferred from the data. For the  $V_p$  model (Figure 1a), its reconstruction only relies on P-P diffracted waves in the ( $V_p, V_s$ ) parameterization, the same as the one in the acoustic FWI, implying why the acoustic FWI can succeed in the  $V_p$  reconstruction when elastic effects have a relatively weak imprint in the data or can be mitigated by a data pre-processing. In contrast, additional S-related wave modes are involved in the  $V_p$  reconstruction for the ( $V_p, R$ ) and ( $V_p, \sigma$ ) parameterizations, making S-waves can also be used to constrain the  $V_p$  reconstruction. Typically, a parameterization with less overlapping of radiation patterns over the scattering angles would be chosen to mitigate the impact of interparameter trade-off in the inversion, such as the ( $V_p, V_s$ ) parameterization where the trade-off only happens in the P-P mode at intermediate scattering angles. However, when inverting the hydrophone data, the introduction of S-related wave modes in the  $V_p$  reconstruction can be vital for avoiding misinterpreting P-to-S-to-P converted waves as P-P reflected waves. For the  $V_s$ -related model, Figure 1b shows parameters of  $V_s, R$  and  $\sigma$  have the same patterns in terms of wave modes and scattering angles, revealing the same data sensitivity. However, their corresponding FWI gradient expressions are different, since gradients for  $R$  and  $\sigma$  consist of contributions from gradients for  $V_p$  and  $V_s$  (Eq. 2). Although this mixture has a negative influence on an isolated  $V_s$  reconstruction, especially for the case that gradient term of  $V_p$  is greater than the one for  $V_s$ , it can create a binding effect from  $V_p$  to stabilize the  $V_s$  reconstruction when data have no/relatively weak energy of reliable S-waves, such as the hydrophone data. Based on the above analysis and the wave dominance in

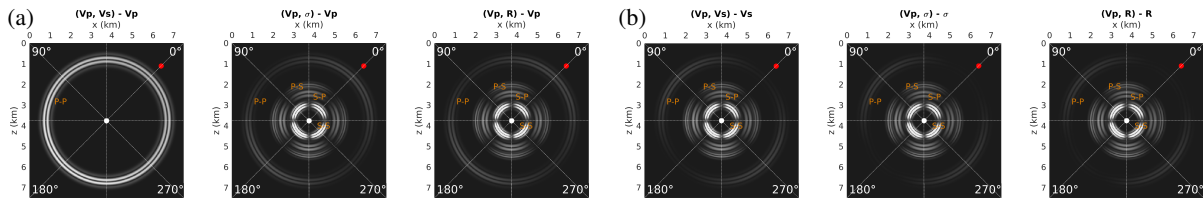


Figure 1: Radiation patterns of the partial derivative wavefield modulus parametrized by  $(V_p, V_s)$ ,  $(V_p, \sigma)$  and  $(V_p, R)$ . (a)  $V_p$  perturbation with fixed  $V_s$ ,  $\sigma$  and  $R$ , (b)  $V_s$ ,  $\sigma$  and  $R$  perturbations with fixed  $V_p$ . The incident source and the parameter perturbation point are denoted in red and white, respectively.

multi-component seismic data, we consider using a two-step hierarchical strategy in elastic FWI:  
 Step 1: Invert P-wave dominated hydrophone data with  $(V_p, R)$  or  $(V_p, \sigma)$  to introduce constraints from converted S-waves in the  $V_p$  reconstruction and stabilize the  $V_s$  reconstruction with the  $V_p$  gradient term;  
 Step 2: Invert S-wave dominated 3C geophone data with  $(V_p, V_s)$  and the resulting  $V_p$  and  $V_s$  from Step 1 as the starting models, where the weak interparameter trade-off in this parameterization contributes to reconstructing  $V_s$  directly from reliable S-waves and mitigating  $V_p$  imprint artifacts.

### Numerical examples

To investigate the feasibility of the proposed two-step hierarchical strategy for multi-component data inversion, we perform FWI tests on two synthetic models with increasing complexity.

In the first example, we use Poisson's ratio  $\sigma$  as the indicator to design a series of 3D overburden models that produce elastic effects varying from weak to strong. As shown in Figure 2a, the main model structure is one high-velocity thick layer overlying a small-scale low-velocity anomaly mimicking a hydrocarbon reservoir. The S-wave velocity models are constructed based on the values of  $V_p$  and  $\sigma$ . Except for the high-velocity overburden, a constant  $\sigma = 0.45$  is used everywhere to build a more natural soft-seabed environment. Different elastic effects are produced at the high-velocity overburden with varying  $\sigma$  from 0.45 to 0.25 (see models  $M_1$  to  $M_5$  in Table 1). A constant density is taken for all those models to make the inversion study focus on the velocity reconstruction. The observed multi-component datasets for models  $M_1 - M_5$  are generated with a 5 Hz Ricker wavelet source-time function and an ocean-bottom node (OBN) acquisition geometry including 20 4C receiver nodes and 25 shooting lines at 5 m water depth (Figure 2a). Figure 2b shows the initial  $V_p$  model, and the initial  $V_s$  model is constructed based on it with a constant  $\sigma = 0.45$ . By applying the two-step hierarchical elastic FWI, Figure 3 displays the  $V_p$  and  $V_s$  profiles obtained at the two stages. Thanks to the additional constraint from converted S-wave modes,  $(V_p, \sigma)$  and  $(V_p, R)$  parameterizations both achieve a robust  $V_p$  reconstruction at Stage 1 for all the models with weak and strong elastic effects (Figure 3a). As a comparison, a  $V_p$  reconstruction with  $(V_p, V_s)$  parameterization is also performed and shows a bias with the elastic effect increasing as indicated by black arrows. The reason can be due to the P-to-S-to-P converted phase occurring at the overburden top edge. When a strong elastic effect exists, the energy of this converted wave can be competitive with the reflected P-waves, making it interpreted as a  $P - P$  reflection mode coming from the overburden bottom edge. Moreover, in Figure 3a, we can also observe how the gradient expressions for  $\sigma$  and  $R$  influence the  $V_s$  reconstruction: the non-linear  $\sigma$  scaling in the  $\sigma$  gradient makes its  $V_s$  model suffer from instability issues in the small  $\sigma$  area, while the  $V_p$  and  $V_s$  gradients mixture in the  $R$  gradient produces a compensation effect from the  $V_p$  model. When moving to Stage 2, the resulting  $V_p$  and  $V_s$  from Stage 1 are used as the starting models, and the final FWI results are shown in Figure 3b. At this stage, the  $V_s$  model is mainly updated compared with the  $V_p$  model, because of the dominance of S-waves and a good separation between P- and S-wave modes in the  $(V_p, V_s)$  parameterization. The  $V_p$  bias of the overburden in strong elastic-effect scenarios from  $(V_p, V_s)$  parameterization is not mitigated by Stage 2, and consequently influences a correct  $V_s$  recover of low-velocity anomaly. In contrast, by combining  $(V_p, R)$  and  $(V_p, V_s)$  parameterizations in the workflow, a robust and reliable  $V_p$  and  $V_s$  joint reconstruction is achieved in both weak and strong elastic-effect scenarios.

The second example is based on the Valhall synthetic model which has a challenging soft-seabed environment and gas cloud with strong elastic effects (extremely low Poisson's ratio). To run with 3D FWI, this 2D model is extended in the  $y$ -direction constantly. The observed multi-component dataset is generated based on the true  $V_p$ ,  $V_s$  and density models illustrated in Figures 4a-4c, using a similar OBN acquisition geometry (19 4C receiver nodes and 16 shooting lines at 5 m water depth) and a 5 Hz Ricker wavelet source-time function. The free-surface boundary condition is applied at the water top.

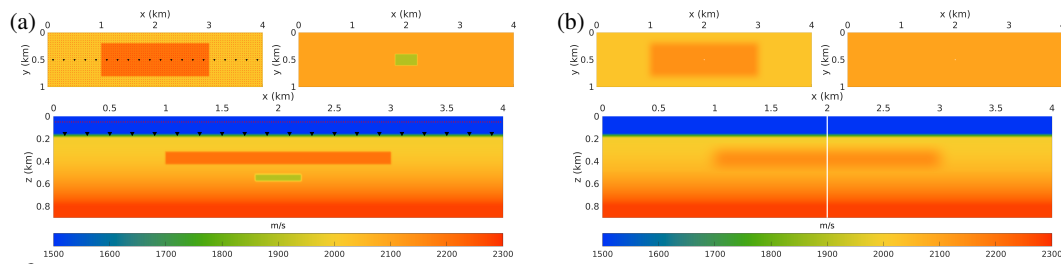


Figure 2: Horizontal and vertical slices of 3D overburden models: true (a) and initial (b)  $V_p$  model. Red dots and black triangles in (a) are shots and OBNs. White line in (b) indicates the location for extracting velocity profile.

To build a more realistic FWI configuration, we remove the energy less than 2.5 Hz in the observed data and estimate the source wavelet from the data based on the initial models (Figures 4d-4f). The two-step hierarchical strategy is used for the  $V_p$  and  $V_s$  model reconstruction, without a density update. Figure 5 illustrates the reconstructed  $V_p$  and  $V_s$  models from two stages, and the results from three different FWI workflows are compared. The details of three FWI workflows are

Stage 1: invert hydrophone data, by three different FWIs: 1) acoustic FWI on primary P waves (Scholte wave and P-to-S-to-P converted wave are muted), 2) elastic FWI with  $(V_p, V_s)$  parameterization on the full data, 3) elastic FWI with  $(V_p, R)$  parameterization on the full data;

Stage 2: invert 3C geophone data (Scholte-wave muted and data weighted by the source-receiver offset to the power of 2), by elastic FWI with  $(V_p, V_s)$  parameterization and different starting models obtained from Stage 1: 1)  $V_p$  from acoustic FWI and initial  $V_s$  in Figure 4e, 2)  $V_p$  and  $V_s$  from elastic FWI with  $(V_p, V_s)$  parameterization, 3)  $V_p$  and  $V_s$  from elastic FWI with  $(V_p, R)$  parameterization.

As expected, after effectively mitigating the elastic effects from the data, the acoustic FWI can be applicable for a reliable  $V_p$  reconstruction, but suffers from oscillating artifacts resulting from a wrong AVO (Figure 4a) and less update in the shallow part due to a sacrifice of near-offset information in the mute, leading to the  $V_s$  reconstruction at the second stage trapped into the shallow part for compensation (Figure 4d). With an elastic approximation, these issues do not appear in  $V_p$  models from two elastic FWIs, and we can find the most robust and reliable  $V_p$  and  $V_s$  reconstruction comes from the workflow with a combination of  $(V_p, R)$  and  $(V_p, V_s)$  parameterizations (Figures 4c and 4f). The  $V_p$  model only using  $(V_p, V_s)$  parameterization shows a similar bias in the gas cloud area (Figure 4b) as in the  $M_5$  overburden model, and consequently impacts the correctness of  $V_s$  reconstruction below it (Figure 4e).

## Conclusions

This study presents the influence of model parameterization and hierarchical design in the elastic FWI of multi-component ocean-bottom data. Three different model parameterizations are analysed from the aspects of the data sensitivity and the model gradient feature. With the help of radiation pattern calculation, the data sensitivity analysis reveals that  $(V_p, R)$  and  $(V_p, \sigma)$  parameterizations provide additional contribution from S-waves to constrain the  $V_p$  reconstruction for interpreting P-to-S-to-P converted waves. The mixture of contributions from gradients for  $V_p$  and  $V_s$  in the  $R$  and  $\sigma$  gradient expressions can create a binding effect from  $V_p$  to stabilize the  $V_s$  reconstruction when data have no/relatively weak energy of reliable S-waves (hydrophone data). When S-wave dominant in the data (geophone data), the  $(V_p, V_s)$  parameterization can focus on the  $V_s$  reconstruction due to its weak trade-off between  $V_p$  and  $V_s$ . Based on those analyses and the wave dominance in the multi-component data, a two-step hierarchical elastic FWI workflow is designed by combining  $(V_p, R)$  and  $(V_p, V_s)$  parameterizations. Its robustness and reliability in the  $V_p$  and  $V_s$  joint reconstruction are illustrated by numerical tests on overburden models with elastic-effect increasing and a realistic Valhall synthetic model.

## Acknowledgements

This study has been partially funded by the SEISCOPE consortium (<http://seiscope2.osug.fr>), sponsored by AKERBP, CGG, CHEVRON, EQUINOR, EXXON-MOBIL, JGI, SHELL, SINOPEC, SISPROBE and TOTAL. This study was granted access to the HPC resources of CIMENT infrastructure (<https://ciment.ujf-grenoble.fr>), Cray Marketing Partner Network (<https://partners.cray.com>) and CINES/IDRIS/TGCC under the allocation 046091 made by GENCI.

## References

- Cao, J., Brossier, R., Górszczyk, A., Métivier, L. and Virieux, J. [2021] 3D multi-parameter full-waveform inversion for ocean-bottom seismic data using an efficient fluid-solid coupled spectral-element solver. *Geophysical Journal International*, **in press**.
- Hamada, G. [2004] Reservoir fluids identification using  $V_p/V_s$  ratio? *Oil & Gas Science and Technology*, **59**(6), 649–654.
- Sears, T.J., Barton, P.J. and Singh, S.C. [2010] Elastic full waveform inversion of multicomponent ocean-bottom cable seismic data: Application to Alba Field, U. K. North Sea. *Geophysics*, **75**(6), R109–R119.
- Wang, H., Burtz, O., Routh, P., Wang, D., Violet, J., Lu, R. and Lazaratos, S. [2021] Anisotropic 3D elastic full-wavefield inversion to directly estimate elastic properties and its role in interpretation. *The Leading Edge*, **40**(4), 277–286.

	$M_1$	$M_2$	$M_3$	$M_4$	$M_5$
$V_p$ (m/s)			2200		
$\sigma$	0.45	0.4	0.35	0.3	0.25
$V_s$ (m/s)	663.33	898.15	1056.85	1175.95	1270.17

Table 1: Physical parameters in the high-velocity overburden of Figure 2a, as used to design the true  $V_s$  models  $M_1$  to  $M_5$ .

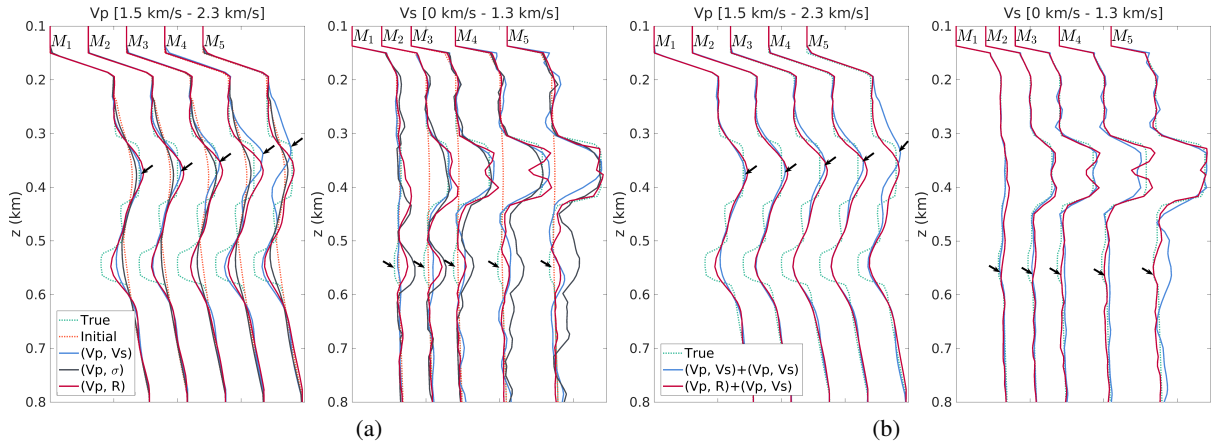


Figure 3: Vertical velocity profiles for comparing the reconstructed  $V_p$  and  $V_s$  of the models  $M_1$  to  $M_5$ . (a) Invert hydrophone data with  $(V_p, V_s)$ ,  $(V_p, \sigma)$  and  $(V_p, R)$  parameterizations, (b) invert 3C geophone data using the  $V_p$  and  $V_s$  from (a) as the starting models, with  $(V_p, V_s)$  parameterization. Anomalies are highlighted by black arrows.

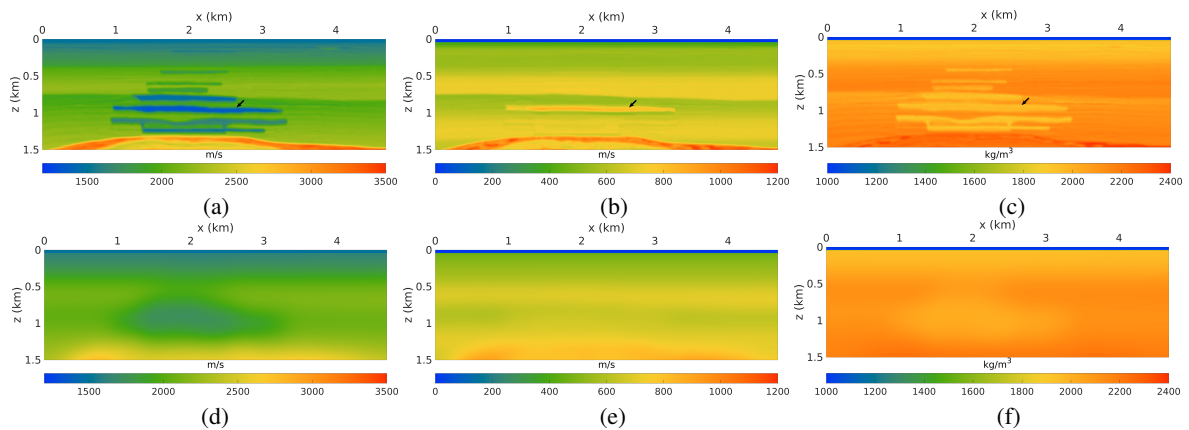


Figure 4: Valhall synthetic models (a, b, c) and corresponding initial models for FWI (d, e, f). Figures from left to right indicate models of  $V_p$ ,  $V_s$  and density, respectively. Black arrows highlight the location of gas cloud which has an extremely low Poisson's ratio ( $\sigma = 0.125$ ) compared with the value of background (around  $\sigma = 0.466$ ).

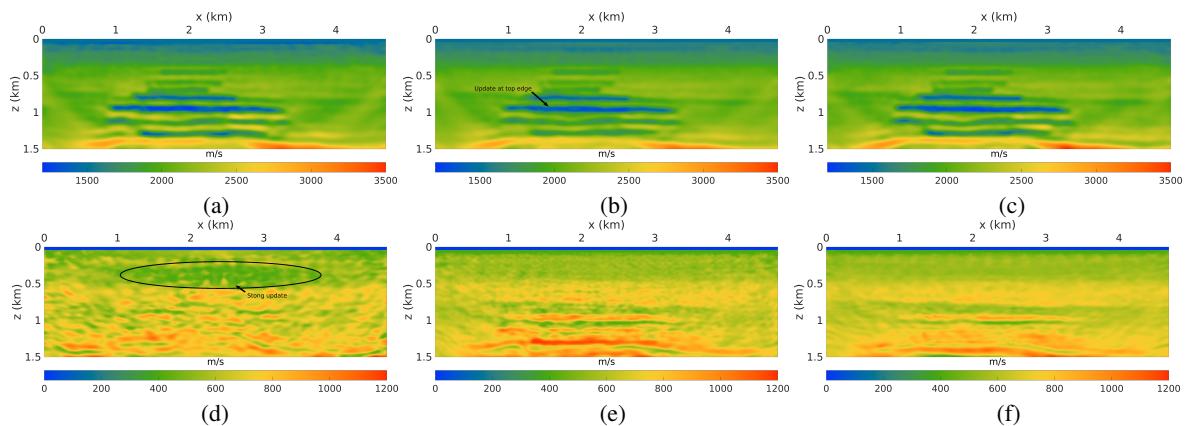


Figure 5: Reconstructed  $V_p$  and  $V_s$  models from three different two-step FWI workflows. Step 1: only invert hydrophone data to get  $V_p$  models using acoustic FWI (a), elastic FWI with  $(V_p, V_s)$  parameterization (b), and elastic FWI with  $(V_p, R)$  parameterization (c), respectively. Step 2: apply elastic FWI with  $(V_p, V_s)$  parameterization to invert 3C geophone data to get  $V_s$  models using the starting models:  $V_p$  in (a) and  $V_s$  in Figure 4e (d),  $V_p$  in (b) together with its updated  $V_s$  from Step 1 (e), and  $V_p$  in (c) and  $V_s = V_p/R$  with the inverted  $R$  from Step 1 (f).